The Enabling Electronic Motif for Topological Insulation in ABO_3 Perovskites

Xiuwen Zhang, Leonardo B. Abdalla, Qihang Liu,* and Alex Zunger**

Stable oxide topological insulators (TIs) have been sought for years, but none have been found; whereas heavier (selenides, tellurides) chalcogenides can be TIs. The basic contradiction between topological insulation and thermodynamic stability is pointed out, offering a narrow window of opportunity. The electronic motif is first identified and can achieve topological band inversion in ABO_3 as a lone-pair, electron-rich B atom (e.g., Te, I, Bi) at the octahedral site. Then, twelve ABO_3 compounds are designed in the assumed cubic perovskite structure, which satisfy this electronic motif and are indeed found by density function theory calculations to be TIs. Next, it is illustrated that poorly screened ionic oxides with large inversion energies undergo energy-lowering atomic distortions that destabilize the cubic TI phase and remove band inversion. The coexistence windows of topological band inversion and structure stability can nevertheless be expanded under moderate pressures (15 and 35 GPa, respectively, for $BaTeO_3$ and $RbIO_3$). This study traces the principles needed to design stable oxide topological insulators at ambient pressures as a) a search for oxides with small inversion energies; b) design of large inversion-energy oxide TIs that can be stabilized by pressure; and c) a search for covalent oxides where TI-removing atomic displacements can be effectively screened out.

1. Introduction

Topological insulators (TIs) are materials having an inverted order of the occupied valence and unoccupied conduction bands at time-reversal invariant wave vectors in the Brillouin zone (BZ), and can be characterized by the non-trivial topological invariant[1,2] $Z_2 = 1$. Theory then assures that in lower-dimensional forms (2D surface or 1D edge) of the topological bulk system, there will be states that possess passivation-resistant, linearly dispersed, and mutually crossing (metallic) energy bands.[3] The required band inversion in the parent bulk system is generally achieved by introducing high atomic number (Z) cations and anions having strong spin–orbit coupling.[4–11] However, such heavy-atom compounds tend to pose defective crystal structures (e.g., spontaneous vacancy formation causing metallic behavior) associated with the relatively low cohesion of the weak heavy-atom chemical bonds.[12–14] The recent quest of topological insulators in oxides[15–21] has been partially motivated by the hope that this will deliver defect-tolerant lattices, often characteristic of metal oxides,[22] while at the same time affording the integration of topological properties with rich oxide functionalities, such as transparent conductivity,[23] ferroelectricity,[24] ferromagnetism,[25] or superconductivity.[26] However, the electronic structures of common octet metal oxides, such as ABO_3 perovskites or A_2BO_4 spinels, show that, while they may be stable and have wide energy band gaps[22] E_g, they generally lack band inversion, having a trivial topological invariant $Z_2 = 0$. For example, the common ABO_3 perovskite have oxygen-derived valence bands and B-atom-derived conduction bands (see **Figure 1**a,b), hence no band inversion. Indeed, whereas numerous topological insulators have been experimentally observed in selenides and tellurides (e.g., Bi_2Se_3[4,7] and Bi_2Te_3[5]), stable oxide TIs are yet unknown: Anecdotal examples abound of theoretically proposed wide-gap oxide TIs in assumed hypothetical crystal structures that turned out, however, to be significantly unstable when energy-lowering structural relaxations were explored in such hypothetical structures.[15–21,27–32]

We conjecture that the conditions needed for topological insulation (i.e., the properties carried by materials that are topological insulators)—depopulation of bonding valence band states and the occupation of antibonding conduction band states—may be contraindicated to thermodynamic stability, if carried out throughout a significant portion of the BZ. If left unscreened (as in strongly ionic systems), such destabilizing forces may drive structural deformations that alter the crystal symmetry and could undo the band inversion, as illustrated below. Although metastable structures can certainly be made,[33–35] it would be desirable to predict compounds that are TIs in not-too-unstable structures, which can be synthesized without the fear of producing a topologically trivial but stabler structure, or decomposing after synthesis to a combination of phases that may not be TIs. In this work, we report the results of ab initio coevaluation of topological insulation and stability for a class of ABO_3 oxide perovskites, elucidating the physical

Prof. X. Zhang, Dr. L. B. Abdalla, Dr. Q. Liu, Prof. A. Zunger
Renewable and Sustainable Energy Institute
University of Colorado
Boulder, CO 80309, USA
E-mail: xiuwen.zhang@colorado.edu; qihang.liu85@gmail.com; alex.zunger@colorado.edu
Prof. X. Zhang
College of Electronic Science and Technology
Shenzhen University
Shenzhen, Guangdong 518060, P. R. China

DOI: 10.1002/adfm.201701266

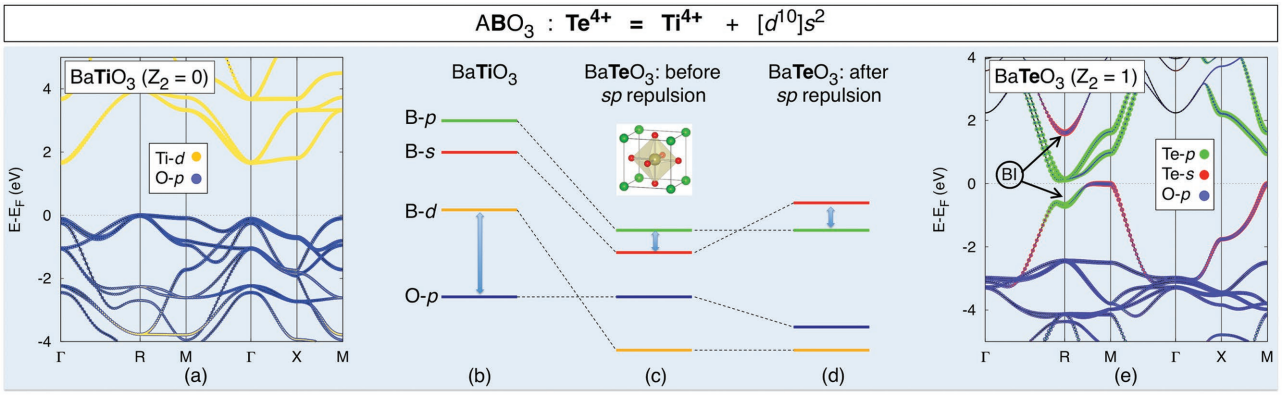

Figure 1. Illustration of the topological gene in cubic ABO_3 by electronic structures in DFT of a) $BaTiO_3$ and e) $BaTeO_3$ with a cubic perovskite (Pm-3m) structure (at zero pressure), and schematic orbital diagram of ABO_3 perovskite compounds, in the cases of b) electron-poor B atom, such as Ti in $BaTiO_3$ where there is no band inversion, and c,d) electron-rich ("lone-pair") B atom, such as Te having additional $d^{10}s^2$ orbital shells, leading to band inversion in $BaTeO_3$. The vertical blue arrows indicate the fundamental band gaps. The inset in (c) shows the "topological gene"—associated with topological insulating character in this class of compounds. BI denotes band inversion with arrows pointing to the inverted states. The dotted lines with different colors denote the band projection onto different atomic orbitals.

origin of the hitherto mysterious difficulty to obtain simultaneously electronic band inversion and thermodynamic stability. We will refer to the electronic structure associated with the geometrical motif shown in Figure 1 (which we will show, enables topological insulation) as the "topological gene." We then identify the topological gene in oxide perovskites as being a lone-pair electron-rich B atom (e.g., Te, I, Bi rather than Ti, Nb, Y, respectively) at the octahedral site in the cubic ABO_3. Oxides tend to have larger predicted inversion energies ($\Delta_i > 1$ eV) than selenides or tellurides ($\Delta_i < 0.4$ eV[5,7]), and are generally less covalent than the heavier chalcogenides where lattice distortions would be partially screened by the more delocalized electronic states. We then illustrate that poorly screened oxide systems with large inversion energies can undergo energy-lowering atomic distortions that remove the topological band inversion. Favorable screening exists in oxides at higher pressures, and lead to stable oxide TIs as illustrated here for $BaTeO_3$ and $RbIO_3$ under moderate pressures. Covalent oxides with strong metal–oxygen orbital mixing[36] do exist and point to the direction of future search for stable oxide TIs at ambient pressures.

2. Previously Proposed Oxide Topological Insulators in Assumed Crystal Structures that are Difficult to Realize or are Unstable

The first theoretically predicted oxide TI $YBiO_3$ was in a Pm-3m structure ($CaTiO_3$-type) with a greatly expanded volume[15] and was later found to transform to a normal insulator upon relaxing its volume and structure to the low-energy phase.[17] Likewise, if one constrains $BaBiO_3$ to be cubic (space group Pm-3m, denoted as S1 in **Table 1**, and moves its Fermi energy E_f up by ≈2e (see the electronic structure of cubic $BaBiO_3$ in **Figure 2**a), equivalent to one added electron per formula unit, or doping by $\approx 10^{22}$ e cm^{-3} and computes the charge density self-consistently, then the system becomes a TI.[16] To examine the effect on stability, we start from the stable form of $BaBiO_3$ (C2/m, denoted as S14 in Table 1 1) rather than the higher energy cubic phase. If we add one electron per formula unit to it in a rigid band approximation (i.e., moving Fermi energy E_f up, no self-consistency allowed), the system is a TI (see Figure 2b). If we actually add a full extra electron per formula unit in the system and allow cell relaxation, the topological band inversion is maintained (see Figure 2c). But, if we iterate this solution to self-consistency (including relaxations of cell-internal atomic positions), the band inversion disappears and the system becomes a normal insulator (see Figure 2d). This shows that the cubically constrained $BaBiO_3$ + e can lower its energy to the S14 structure if the constraints on relaxation are removed and it lose its topological character. A similar situation applies to cubic $RbTlCl_3$[28] and $KBiO_3$.[18]

Table 1. Crystal structures of the studied ABO_3 compounds.

Label	Prototype compound	Space group	ICSD number
S1	$CaTiO_3$	Pm-3m	162924
S2	$RbIO_3$	R3m	2825
S3	$GdFeO_3$	Pnma	154065
S4	$KClO_3$	$P2_1/m$	26408
S5	$BaTeO_3$	$P2_1/c$	None[a]
S6	$SrTeO_3$	P1	74396
S7	$CaTeO_3$	$P2_1$	260238
S8	$CaSeO_3$	$P2_1/c$	159880
S9	KIO_3	R3	424864
S10	$NaBrO_3$	$P2_13$	47174
S11	$GaBiO_3$	Pcca	171709
S12	$AlBiO_3$	P1	None[b]
S13	$ScBiO_3$	P1	None[b]
S14	$BaBiO_3$	C2/m	172757
S15	$SrBiO_3$	$P2_1/c$	85173

[a] Recently synthesized structure used in this work; [b] Predicted in ref. [17].

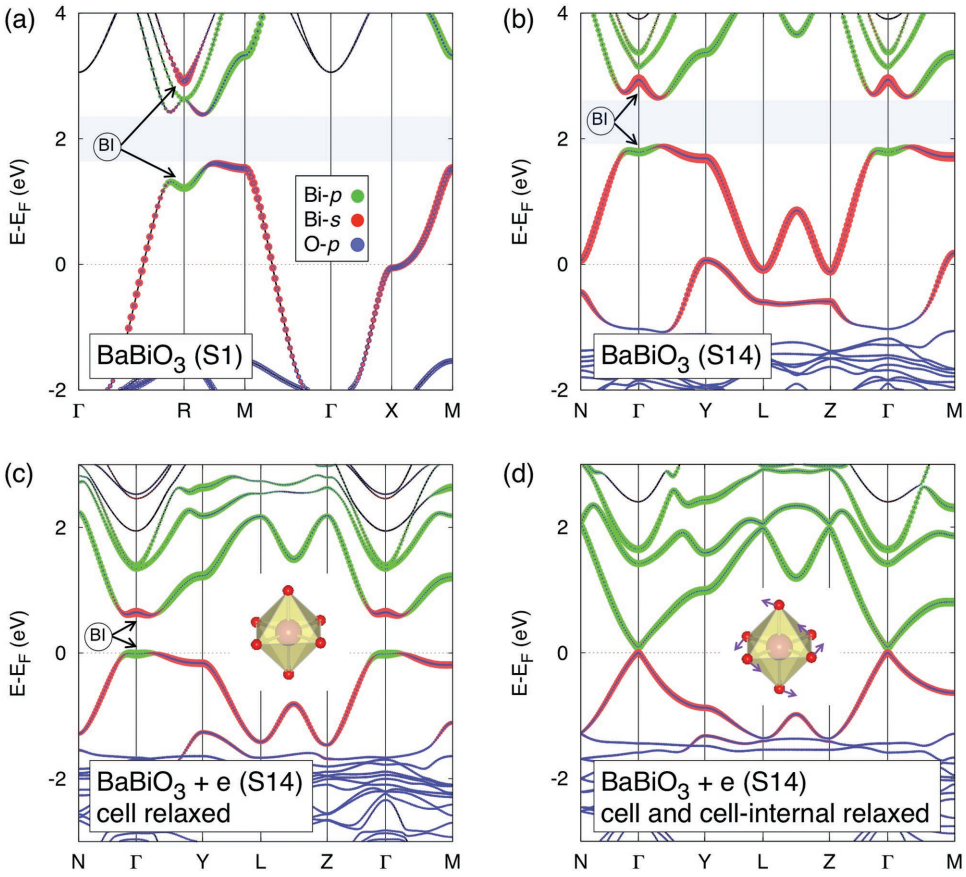

Figure 2. Electronic structures of $BaBiO_3$ in a) the cubic S1 (Pm-3m) structure or b) the experimentally observed S14 (C2/m) structure, showing the excited-state band inversions (for the energy gap indicated by blue backgrounds). c,d) Electronic structures of $BaBiO_3$ + e (doped artificially by one electron per formula unit) in S14 structure (cell shape relaxed) before (c) or after (d) cell-internal atomic displacements (at zero pressure). The band inversion is denoted in the figure by BI, with arrows pointing to the inverted states. The dotted lines with different colors denote the band projection onto different atomic orbitals.

There are also some 2D oxides that have been predicted theoretically to be TIs in hypothetical structures.[19–21] Examples include the assumed (111) bilayers of $LaAuO_3$ and $SrIrO_3$ compounds, which, however, were shown to undergo TI to antiferromagnetic insulator transition.[20] Similarly, a single monolayer of ZrSiO, assumed to be exfoliated from its stable 3D layered form, has recently been predicted to be a topological insulator.[21] However, given the large calculated binding energy >1 eV of the 2D ZrSiO monolayer to its bulk 3D lattice,[21] one would doubt if the isolated 2D layer could be stabilized. Another topological property (Dirac semimetal) was theoretically illustrated[29] in BiO_2 in the assumed β-cristobalite (SiO_2) structure (forcing a 4+ oxidation state on Bi); however, its stable experimental structure[30] (β-Sb_2O_4-type, C2/c, a charge ordered structure with stable oxidation states 3+ and 5+ of Bi) that has much lower total energy than β-cristobalite BiO_2,[31,32] is a normal insulator.

3. Topological Gene and Stability Gene

To address the issue of possible conflict between band inversion and stability, we introduce two constructs: We first identify an electronic motif within a group of ABO_3 oxides that would generate band inversion—the "topological gene" of this group of compounds. As Figure 1c,d illustrates, the topological gene here is the octahedral BO_6 motif with lone-pair B atom (generated, e.g., by replacing an electron-poor Ti atom in $BaTiO_3$ by an electron-rich Te atom in $BaTeO_3$ that has an additional $d^{10}s^2$ shell). Second, we examine the stability of the crystal structure that hosts the topological gene, relative to the ground state structures that hosts the "stability gene" of this group of compounds. The key challenge is to see if structures with the topological gene can also have the stability gene. Thus, coevaluation of the electronic structure and stability is required.[37]

We confirm via calculated band structures in the framework of density function theory (DFT) using projector-augmented wave (PAW) pseudopotential with the exchange-correlation of Perdew–Burke–Ernzerhof (PBE)[38–40] and the calculated topological invariant[41,42] Z_2 (see the Experimental Section and Section SI in the Supporting Information for the details of calculation methods). Section SII (Supporting Information) provides the values of the excitation gaps, as well as lattice parameters of the studied crystal structures.

We find that 12 ABO_3 compounds ($BaTeO_3$, $SrTeO_3$, $CaTeO_3$, $BaSeO_3$, $SrSeO_3$, $CaSeO_3$, $RbIO_3$, KIO_3, $NaIO_3$, $RbBrO_3$, $KBrO_3$,

$NaBrO_3$) in the assumed cubic perovskite structure with lone-pair B atoms at the octahedral site are in fact TIs, whereas the corresponding compounds with non-lone-pair B ions at the octahedral site (e.g., $BaTiO_3$ and $KNbO_3$) are found to be normal insulators. This substantiates the identity of the topological gene in ABO_3 compounds. Section SIII (Supporting Information) discusses the excitation gaps in the compounds designed according to the topological gene, and the effects due to possible DFT errors as compared to hybrid functional (in Heyd-Scuseria-Ernzerhof form, or HSE06[43]) calculations. The results show that the inversion energy (Δ_i), i.e., the energy difference between the inverted valence and conduction bands at time-reversal invariant wave vectors, is slightly reduced (by 4%) in HSE06 as compared to DFT, indicating that the band inversion discussed here is quite robust against DFT errors.

We find, however, that the crystal structure that hosts this topological gene is not the stablest structure at this composition: total energy relaxation calculations reveal that the cubic topological structures would relax to lower energy noncubic perovskite phases that are not TIs. Indeed, by performing constrained DFT calculations (see the Experimental Section), we observe a regained stability of the cubic phase. We further identified the window of coexistence of topological insulation and stability at ambient conditions, and find that the topological cubic ABO_3 phases have inversion energies lying outside this coexistence window. Building upon this identification, we find that moderate external pressure can significantly expand the above coexistence window, and eventually leads to simultaneously stable and topological cubic ABO_3 phases, thus bringing the "stability gene" into coincidence with the "topological gene."

4. Electronic Requirements for the Topological Gene in Cubic ABO_3 Perovskites

In conventional ABO_3 compounds with electron-poor B atoms (such as illustrated in Figure 1b), the occupied valence band is oxygen derived whereas the empty conduction states are B-atom derived with normal, *s*-below-*p* orbital order (thus, no inversion). To induce band inversion, one would like to change the order of B atom orbitals to *p*-below-*s* and assure that the Fermi energy is located between these occupied and unoccupied states, respectively. The idea is to replace the B atom in ABO_3 in the cubic perovskite structure (see the inset of Figure 1c) by an electron-rich B element of the same formal charge. Such a B atom has an occupied (lone-pair) *s* orbital below its empty *p* orbital, yet above the O-*p* state, as shown in Figure 1c. The lone-pair *s* orbital can thus become an unoccupied state above the conduction band due to (B-atom *s*)–(oxygen *p*) level repulsion, leading to band inversion (B-*p* below B-*s*) as well as to a finite excitation band gap between B-*p* (occupied) and B-*s* (unoccupied), which is illustrated in Figure 1d. We will illustrate via quantitative DFT calculations the above concept and its rather broad applicability for different groups of perovskite compounds.

4.1. Cubic $BaTeO_3$ is a TI Whereas Cubic $BaTiO_3$ is Not

In the II_A-IV_A-O_3 group of compounds exemplified by $BaTiO_3$, we replace Ti^{4+} by the electron-richer Te^{4+} having additional $d^{10}s^2$ shell, leading to the II_A-VI_B-O_3 group of compounds exemplified by $BaTeO_3$. Two effects, noted by our detailed DFT calculations and illustrated by a simple orbital diagram (see Figure 1) are associated with this transmutation: i) Because of the addition of $d^{10}s^2$ shell (where the s^2 lone-pair band is occupied), the outmost B-*d* and B-*s* states of B = Te become occupied, with a band gap located between B-*s* and B-*p* states (see Figure 1c,d). The outer *s*, *p*, and *d* atomic orbitals of B = Te drop in energy relative to B = Ti (because of the less screening of the core by the valence shell). ii) The relativistic Darwin[44] effect causes the *s* orbital to become relatively localized and introduce an occupied lone-pair *s*-band, which in this case lies above the O-*p* bands. Since in the cubic perovskite structure Te (in $BaTeO_3$) or Ti (in $BaTiO_3$) are located at the octahedral O_h site where they are bonded to six O atoms, there will be a level repulsion between the O-*p* and Te-*s* bands, displacing the Te-*s* band upward. If the repulsion is strong enough, as it is at the R point in the BZ (see Figure 1e), this repulsion will place Te-*s* above Te-*p* (see Figure 1d), leading to band inversion between Te-*s* and Te-*p* states at R point in the Pm-3m structure (labeled as S1 in Table 1). Therefore, the use at the B site of the electron-rich version (Te in place of Ti) causes band inversion, thus constituting the topological gene in these systems.

Figure 1a,e illustrates this design principle via DFT band structure. We see that while in $BaTiO_3$, the conduction band minimum (CBM) is composed of Ti-atom 3*d* states (yellow) throughout the BZ, in $BaTeO_3$ there is a band inversion at R point where the valence band maximum (VBM) is made of Te-*p* orbital (green) instead of Te-*s* orbital (red). Calculation of the topological invariant from the wavefunctions (see the Experimental Section) finds $Z_2 = 1$ in $BaTeO_3$ as compared to the expected $Z_2 = 0$ in $BaTiO_3$. That this design principle is rather general can be seen by considering other leading ABO_3 perovskite prototypes.

4.2. Cubic KIO_3 is a TI whereas $KNbO_3$ is Not

In the I_A-V_A-O_3 group of compounds exemplified by $KNbO_3$, we replace Nb^{5+} by I^{5+} leading to the group I_A-VII_B-O_3 exemplified by KIO_3. We find $Z_2 = 0$ in $KNbO_3$ whereas $Z_2 = 1$ in KIO_3. **Figure 3** shows the electronic structures of $KNbO_3$ and KIO_3. We see that while in $KNbO_3$ the CBM is composed of Nb-atom 3d states (yellow) throughout the BZ, in KIO_3 there is a band inversion at R point where the VBM is made of I-*p* orbital (green) instead of I-*s* orbital (red). Calculation of the topological invariant finds $Z_2 = 1$ in KIO_3 and $Z_2 = 0$ in $KNbO_3$.

5. Band Inversion is Often Contraindicated to Stability

Having identified and verified an electronic motif—the topological gene—we next ask whether the crystal structure (here, cubic ABO_3 perovskite) that harbors the topology coincides with the structure that harbors stability.

Figure 4 shows the total energies (in meV per atom, given in parentheses) of various ABO_3 structures (denoted S1–S15 in Table 1, S1 being the cubic perovskite structure while S2–S15

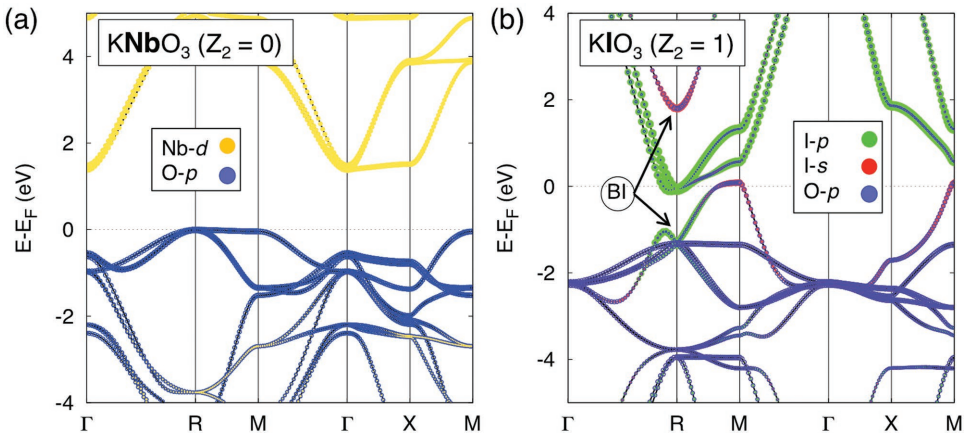

Figure 3. Electronic structures in the cubic perovskite (Pm-3m) structure of $KNbO_3$ with a) electron-poor BO_6 or b) KIO_3 with electron-rich BO_6 octahedra (at zero pressure). BI denotes band inversion. The dotted lines with different colors denote the band projection onto different atomic orbitals.

being the lowest-energy structures of specific ABO_3 compounds), relative to the lowest-energy phase. The A position in ABO_3 with the S1 (prototype compound: $CaTiO_3$) structure is the cube vertices (Ca sites in $CaTiO_3$) and the B position is part of the BO_6 octahedra (Ti sites in TiO_6 of $CaTiO_3$), similarly for S2–S15 types. We considered the swapping of A and B elements on the ABO_3 atomic site to create BAO_3, and found that this lowers the energy for 33 structures in our calculations, which are marked by italics text in Figure 4, meaning that the lowest energy structure is BAO_3. The lattice parameters (as well as band gaps) of the relaxed crystal structures in Figure 4 are provided in Table S1 (Supporting Information). In addition to stability, Figure 4 also denotes if according to the calculated topological invariant Z_2 the compound is a TI or a normal insulator. We find from such total energy minimizations that the BO_6 octahedral unit with the said electron rich B atom tends to distort toward a stabler, noncubic crystal structure[31,32] and that this distortion removes the topological insulation. Therefore, the stability gene and TI gene tend to contradict each other for the ABO_3 compounds at ambient conditions: ABO_3 oxides that are stable are not TIs and structures that are TIs are not stable.

VI$_B$ / II$_A$	Te	Se
Ba	$BaTeO_3$ S1 (156) : R^1 *S2 (76):* *NI* *S3 (37):* *NI* S4 (3): NI S5 (0): NI	$BaSeO_3$ S1 (366) : R^1 S2 (75) : NI *S3 (63) :* *NI* S4 (0) : NI
Sr	$SrTeO_3$ S1 (232) : R^1 *S2 (43) :* *NI* S4 (14) : NI S6 (9) : NI *S3 (0) :* *NI*	$SrSeO_3$ S1 (353) : R^1 *S2 (68) :* *NI* *S3 (25) :* *NI* S4 (0) : NI
Ca	$CaTeO_3$ S1 (426) : R^1 S4 (76) : NI *S2 (52) :* *NI* *S3 (17) :* *NI* S7 (0) : NI	$CaSeO_3$ S1 (449) : R^1 *S2 (46) :* *NI* S4 (46) : NI *S3 (12) :* *NI* S8 (0) : NI

VII$_B$ / I$_A$	I	Br
Rb	$RbIO_3$ S1 (241) : R^1 *S3 (37) :* *NI* S4 (24) : NI S2 (0) : NI	$RbBrO_3$ S1 (551) : R^1 *S3 (20) :* *NI* S4 (5) : NI S2 (0) : NI
K	KIO_3 S1 (190) : R^1 *S3 (22) :* *NI* S4 (21) : NI S2 (6) : NI S9 (0) : NI	$KBrO_3$ S1 (476) : R^1 *S3 (9) :* *NI* S2 (3) : NI S4 (0) : NI
Na	$NaIO_3$ S1 (224) : R^1 *S2 (56) :* *NI* *S4 (34) :* *NI* *S3 (0) :* *NI*	$NaBrO_3$ S1 (469) : R^1 *S2 (51) :* *NI* S4 (36) : NI *S3 (7) :* *NI* S10 (0) : NI

A / G.	Ga/Y/Ba	Al/Sc/Sr
III$_B$	$GaBiO_3$ *S1 (223):* *NI* *S2 (76) :* *NI* *S3 (71) :* *NI* S4 (48) : NI S11 (0) : NI	$AlBiO_3$ *S1 (97) :* *NI* *S4 (81) :* *NI* *S3 (44) :* *NI* *S2 (38) :* *NI* S12 (0) : NI
III$_A$	$YBiO_3$ *S1 (629):* *NI* S4 (39) : NI *S2 (31) :* *NI* *S3 (0) :* *NI*	$ScBiO_3$ *S1 (325):* *NI* S4 (77) : NI *S2 (27) :* *NI* *S3 (10) :* *NI* S13 (0) : NI
II$_A$	$BaBiO_3$ (+e) S4 (76) : NI S1(23) : R^1 S3 (4) : Γ^1 S14 (0) : Γ^1	$SrBiO_3$ (+e) S1(142): R^1 S2 (119): Z^1 S4 (69) : NI S3 (14) : Γ^1 S15 (0) : Γ^1

Figure 4. Presence of topological properties (indicated by red, with R^1 denoting the single band inversion at R point in the BZ, similarly for Z^1 and Γ^1) versus absence (indicated by black, with NI denoting normal insulator) and relative DFT total energies (meV per atom, with zero indicating the ground state, shown in parentheses) of ABO_3 compounds with different crystal structures S1–S15 (see Table 1) at zero pressure. The A and B positions are the cube vertices and part of the BO_6 octahedra, respectively. We considered the swapping of A and B elements on the ABO_3 atomic site, i.e., BAO_3, and marked by italics text if the lowest energy structure is BAO_3. All considered compounds except $YBiO_3$, $ScBiO_3$, $GaBiO_3$, and $AlBiO_3$ (note that in their lower-energy S1 structure, Bi is at the A site), are thermodynamically stable in their lowest-energy structure, as found by DFT calculations of the convex hull.[31,32] The initial S2 structure of $BaBiO_3$ relaxes into the S1 structure, thus the total energy of S1 but not S2 structure is reported. For $BaBiO_3$ and $SrBiO_3$, we calculate the band inversion after doping by one electron/formula unit (rigidly moving Fermi level up; denoted by "(+e)"). For other compounds, we calculate the band inversion at the band edges.

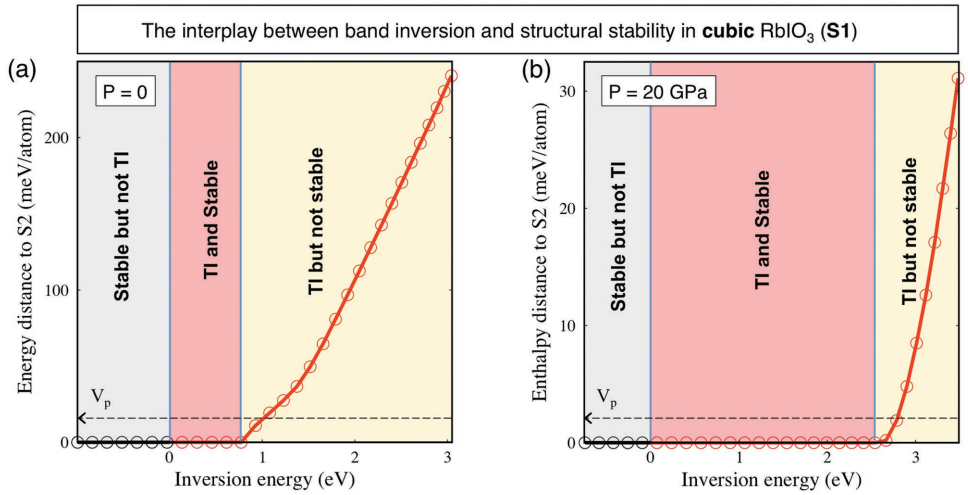

Figure 5. Illustration of the interplay between band inversion and structural stability in cubic $RbIO_3$ at a) 0 GPa and b) 20 GPa. The inversion energy in the cubic system is tuned by applying an external potential (V_p; $V_p = 0$ corresponds to the largest inversion energy) (see the evolution of electronic structures with decreasing inversion energy for 0 and 20 GPa in Figures S8 and S9 (Supporting Information), respectively).

6. Model DFT Calculation of the Evolution of the Electronic Structures with Decreasing Inversion Energy

To get a deeper understanding on the interplay between structural stability and band inversion, we perform constrained DFT calculations constructed for tuning band inversion to examine its effect on the total energy. The tuning of the inversion energy can be done by using an external potential that shifts upward the B atom p orbital energy, thus, according to Figure 1d, the inverted structure (*p*-below-*s*) can be tuned to be uninverted (*s*-below-*p*). This constraint can be implemented, for example, by adding an external potential term[45] V_p to the DFT Hamiltonian acting on the I-*p* orbital in $RbIO_3$. We then monitor the total energy of the cubic perovskite structure (S1) relative to its stable R3m rhombohedral phase (S2 in Table 1) as a function of Δ_i. **Figure 5**a shows that as Δ_i decreases, the energy of the cubic S1 phase (relative to S2) also decreases, indicating that band inversion is contraindicated with the stability of crystal structure.

Figure 6 illustrates the evolution of band structures of cubic $RbIO_3$ with inversion energies tuned by V_p, demonstrating that as the inversion energy decreases (V_p increases), the I-*p* states moves up relative to the I-*s* states and the *p*-below-*s* band inversion is gradually removed. The method of adding to the Hamiltonian an external potential V_p to independently control the band inversion is a useful device for answering the question of whether the band inversion energetically drives the structural distortions, or whether other factors drive the structural distortions and the band inversion is removed only as a side effect (it is the former). However, we remind the reader that this potential term does not represent an actual material. Figure 6c shows the band structure of cubic $RbIO_3$ with a rather large inversion-energy (0.8 eV) where band topology and structural stability coexist, from which we see that the inverted bands are rather dispersive, leaving most of the BZ uninverted. On the contrary, as shown in Figure 2c, $BaBiO_3$ S14 structure (see Table 1) has a smaller Δ_i (≈0.7 eV) but a larger area of the BZ with band inversion due to smaller band dispersions compared to those in Figure 6c, and thus undergoes atomic displacement that removes the band inversion. This suggests that the depopulation (occupation) of bonding valence (antibonding conduction) band states induced by band inversion, if throughout a significant portion of the BZ, is contraindicated to the stability of the structure that hosts the band inversion.

Significantly, however, there is a narrow window ($0 < \Delta_i <$ 0.8 eV) shown by red background in Figure 5a, where topological band inversion and the stability of the band-inverted crystal structure can coexist. It is noticed that the currently known stable TIs (e.g., Bi_2Se_3[7] and Bi_2Te_3[5]) have Δ_i much smaller than 0.8 eV, lying inside the coexistence window ($0 < \Delta_i <$ 0.8 eV). Whereas, the cubic ABO_3 structures with short B—O bonds have $\Delta_i > 1$ eV due to the strong coupling between B-*s* and O-*p* states, lying outside of the coexistence window. Instead of searching for stable oxide TIs with small Δ_i, we attempt to stabilize oxide TIs with large inversion energies.

7. Bringing the Topological Gene into Overlap with the Stability Gene by Applying Pressure

Inspired by the fact that many ABO_3 compounds (e.g., $BaTiO_3$[46]) that are not cubic at ambient conditions can be stabilized under external pressure in the cubic form, we test the effect of external pressure on the interplay between band inversion and structural stability. We perform similar calculations as Figure 5a, but apply external hydrostatic pressure of ≤20 GPa. The result of Figure 5b shows that the coexistence window for band inversion and structural stability (red background) is significantly extended. At 20 GPa, a stable TI structure can form while tolerating a band inversion of the magnitude of about 2.5 eV. To demonstrate the dramatic effect of pressure on topological insulation versus stability diagram (Figure 5b), we perform enthalpy calculations for $BaTeO_3$ (from group II_A-VI_B-O_3) and $RbIO_3$ (from group I_A-VII_B-O_3). **Figure 7**a,b shows the calculated enthalpies of the relevant structure types for $BaTeO_3$ and $RbIO_3$, as a function of hydrostatic pressure, which

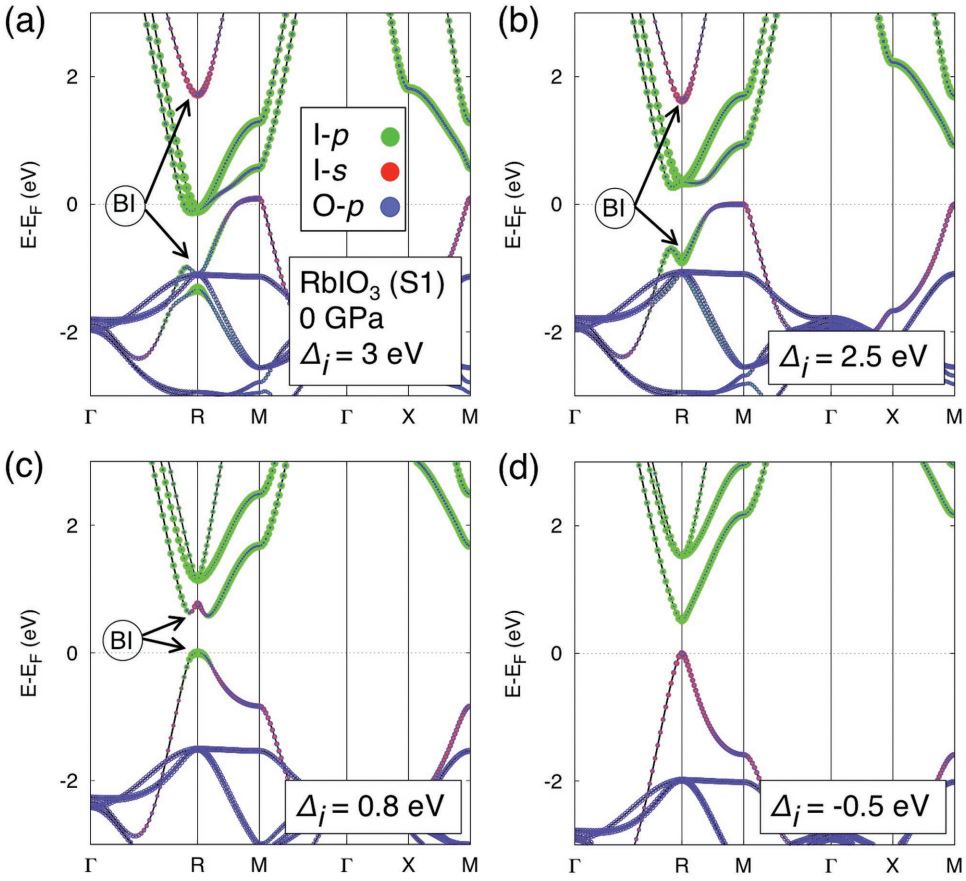

Figure 6. Electronic structures of cubic $RbIO_3$ (S1) at zero pressure versus tuned (by the Hubbard-like term V_p) inversion energy of a) ≈3 eV (V_p = 0), b) ≈2.5 eV (V_p = 6 eV), c) ≈0.8 eV (V_p = 19 eV), or d) ≈–0.5 eV (V_p = 27 eV). BI denotes band inversion. The dotted lines with different colors denote the band projection onto different atomic orbitals.

demonstrate that the cubic perovskite (S1, see red squares in Figure 7a,b) tends to be stabilized by external pressure. At pressure of 15 GPa (35 GPa), the S1 phase that contains the topological gene becomes the lowest-enthalpy structure for $BaTeO_3$ ($RbIO_3$). We further check the effect of external pressure on the band inversions in cubic $BaTeO_3$ and $RbIO_3$, finding that the band inversion is not removed by external pressure (see Figure 7c,d), but on the contrary, increased by the pressure from 2.3 eV at 0 GPa to 3.4 eV at 35 GPa for $BaTeO_3$, and from 3.0 eV at 0 GPa to 3.8 eV at 35 GPa for $RbIO_3$. It is expected because the pressure decreases the atomic bond lengths of BO_6 octahedra, leading to larger *s*–*p* repulsion. The enhanced tolerance of cubic ABO_3 structures to band inversions is because of the increased electronic screening effect under pressures. The topological phases under pressure are usually metallic (see, e.g., Figure 7c,d) even for $BaTeO_3$ that has a nonzero band gap at zero pressure (see Figure 1e). We emphasize that the predictions regarding pressure effects are directed toward illustrating the physical principle of coexistence of stability and topological character, rather than producing a technologically viable gapped system. Similar to heavier-chalcogenide TIs (e.g., Bi_2Se_3), the lattice distortions would be screened by the delocalized electronic states. Here, we use external pressure (as an example of external constraints) to tune the screening effect in oxides. Strong screening could exist in oxides without external constraints, such as covalent oxides with strong metal–oxygen orbital mixing,[36] pointing to the direction of future search of stable oxide TIs with large inversion energies that is robust under perturbations such as thermal expansion.

8. Conclusions and Discussion

The last years have witnessed intense search of ABX_3 chalcogenide TIs but have thus far failed to discover stable oxide TI whereas other chalcogenides can be TIs. This is unfortunate, because oxides have many other properties that could ideally combine with topological insulation. We point to the fact that band inversion in a significant portion of the BZ might be contraindicated to thermodynamic stability as this generally means depopulating valence band bonding states and populating the higher kinetic energy antibonding conduction states. Such an effect can be tolerated thermodynamically only if it occurs with small enough inversion energy over a small part of the BZ. We note that many stable topological insulators with inversion energies less than 0.8 eV have been found experimentally in non-oxide chalcogenide systems (e.g., Bi_2Se_3 with inversion energy <0.4 eV), but not oxides. The inversion energies in ABO_3 oxides are typically larger than 1 eV at ambient conditions. The reason that band-inverted non-oxide chalcogenides tend to be less

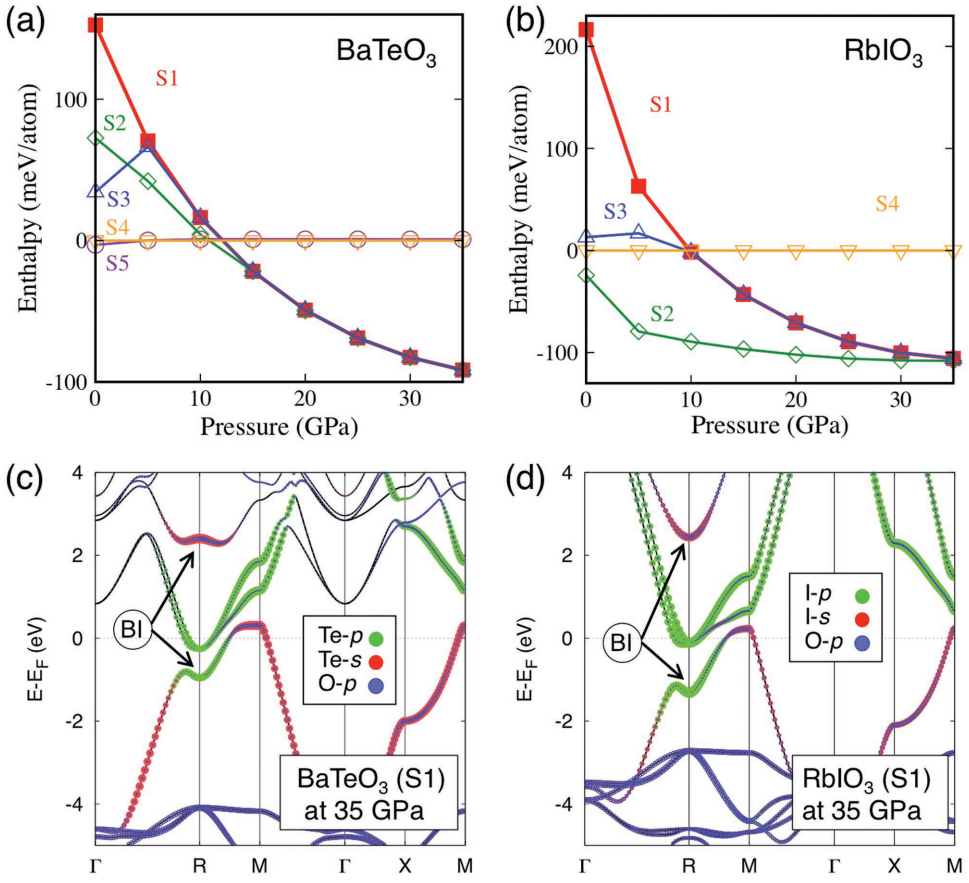

Figure 7. Enthalpies of a) $BaTeO_3$ and b) $RbIO_3$ in the ABO_3 structures as functions of pressure, illustrating that the cubic perovskite structure (S1) with the topological gene becomes the lowest-enthalpy structure at moderately high pressure. For graphic clarity, the enthalpies of the S4 structures ($P2_1/m$) are chosen as the zero at each pressure. Swapping of A and B sites has been considered, and the lowest-energy configuration is selected. c,d) Electronic structures of cubic $BaTeO_3$ (c) and $RbIO_3$ (d) under external pressure of 35 GPa. The band inversion is denoted in the figure by BI, with arrows pointing to the inverted states. The dotted lines with different colors denote the band projection onto different atomic orbitals.

unstable than band-inverted oxides is because destabilizing band inversion drives structural distortions that often remove the topological gene (as illustrated in our examples $RbIO_3$, $BaTeO_3$), but such distortions can be effectively screened if the material is not too ionic and its electronic states are delocalized, as is the case in heavier non-oxide chalcogenides. In oxides, such covalence induced screening may require pressure. However, covalent oxides with strong metal–oxygen orbital mixing[36] do exist and might be a fruitful platform for searching for oxide TIs.

The future challenge is to find oxide compounds that overcome the general conflicting trends between topological insulation and stability. This defines a design principle, deciding what one needs to look for, and clarifies that whereas finding such a "window of opportunity" is possible in principle, it involves a delicate balance that was not achieved thus far—except in the appearance of external constraints (moderate pressure), as shown here as a "proof of principle" of our main insight. The results in this study also suggest the directions for future search of stable oxides TIs: a) search for oxides with small inversion energies; b) design of large inversion-energy oxide TIs that can be stabilized by external constraints or intrinsic screening effect; and c) search for covalent oxides where TI-removing atomic displacements can be effectively screened out.

9. Experimental Section

DFT Total Energy and Electronic Structure Evaluation: Total energies were calculated using the PAW pseudopotential[40] total energy method without spin–orbit coupling with the exchange-correlation of PBE[38] as implemented in the Vienna ab initio simulation package (VASP).[39] An energy-cutoff of 520 eV and reciprocal space grids with densities of $2\pi \times 0.068$ and $2\pi \times 0.051$ Å^{-1} for relaxation and static calculation, respectively, were used. Electronic structure and physical properties were calculated from DFT, taking into account spin–orbit coupling by a perturbation $\sum_{i,l,m} V_l^{SO} \vec{L} \cdot \vec{S} \, |l,m\rangle_{i\,i} \langle l,m|$ to the pseudopotential[47] ($|l, m\rangle_i$ is the angular momentum eigenstate of atomic site i. To illustrate the band inversions, the calculated wave function $|\varphi\rangle$ was projected on spin and orbital basis of each atomic site $C_{i,l,m,\eta} = \langle \varphi \, | (s_\eta \otimes |l,m\rangle_{ii} \langle l,m|) | \varphi \rangle$ and then $C_{i,l,m,\eta}$ was summed for a given atomic orbital. The Wigner–Seitz radii for constructing $|l, m\rangle_i$ used in this study are listed in the pseudopotentials of the VASP simulation package.[39] To illustrate the interplay between band inversion and structural stability, constrained DFT calculations were performed by applying a Hubbard-like external potential term[45] (V_p) on the I-p orbital in $RbIO_3$ in the Hamiltonian to gradually remove the band inversion between I-p and I-s states.

Z_2 Characterization: For centrosymmetric structures, Z_2 was evaluated from the parities of the wave functions at the time reversal invariant k-points.[42] For non-centrosymmetric structures, the method from refs.[2,41,48] was used to calculate the topological invariant Z_2, which is based on the evolution of Wannier function centers. The topological

invariant Z_2 is expressed as the number of times mod 2 of the partner switching between the Wannier function centers during the evolution (as illustrated in Figure S1 in the Supporting Information). To directly look at the evolution of Wannier function centers, the scheme proposed by Yu et al. was followed.[41] The topological nature of a 3D compound is determined by looking at two effective 2D systems with $k_z = 0$ and $k_z = \pi$. Each 2D effective system is then considered as a series of effective 1D system with fixed k_y. For an effective 1D system with periodic condition, the unitary position operator is defined as

$$\hat{x} = \sum_{j\alpha} e^{-i\delta_{k_x}\cdot R_j} \left| j\alpha \right\rangle \left\langle j\alpha \right| \tag{1}$$

where $\delta_{k_x} = \frac{2\pi}{N_x a_x}$, N_x is the number of real space unit cells along x direction, R_j denotes the position of the jth lattice site, and α denotes the index of the Wannier function $|j\alpha\rangle$. The projection operator for the occupied subspace for a fixed k_y can be defined as

$$\hat{P}_{k_y} = \sum_{n\leq 2N, k_x} \left| \psi_{nk} \right\rangle \left\langle \psi_{nk} \right|; \quad \text{for } k_z = 0 \text{ or } k_z = \pi \tag{2}$$

where $|\psi_{nk}\rangle$ is the Bloch state and $2N$ is the number of occupied states.

The eigenvalue of the projected position operator was then considered

$$\hat{x}_P\left(k_y\right) = \hat{P}_{k_y}\, \hat{x} \hat{P}_{k_y} \tag{3}$$

that has the following form

$$\hat{x}_P(k_y) = \begin{bmatrix} 0 & X_{0,1} & 0 & 0 & \cdots & 0 \\ 0 & 0 & X_{1,2} & 0 & \cdots & 0 \\ 0 & 0 & 0 & X_{2,3} & \cdots & 0 \\ \vdots & \vdots & \vdots & \vdots & \vdots & \vdots \\ 0 & 0 & 0 & 0 & \cdots & X_{N_x-2,N_x-1} \\ X_{N_x-1,0} & 0 & 0 & 0 & \cdots & 0 \end{bmatrix}, \tag{4}$$

where $X_{0,1}$, $X_{1,2}$, ... are $2N \times 2N$ matrices. The eigenvalue of the projected position operator can be solved by the transfer matrix method. A product of $X_{0,1}$, $X_{1,2}$, ... was defined as

$$D\left(k_y\right) = X_{0,1} X_{1,2} X_{2,3} \cdots X_{N_x-2,N_x-1} X_{N_x-1,0} \tag{5}$$

$D(k_y)$ has $2N$ eigenvalues

$$\lambda_m^D\left(k_y\right) = \left|\lambda_m^D\left(k_y\right)\right| e^{i\theta_m^D(k_y)}, m = 1,\ldots 2N \tag{6}$$

The evolution of the Wannier function center with k_y can be easily obtained by looking at the phase factor θ_m^D (named Wannier center for convenience). The Wannier centers are paired at $k_y = 0$ and $k_y = \pi$, and during the evolution from $k_y = 0$ to $k_y = \pi$, the Wannier center can switch partners, with an odd number of partner switching corresponding to $Z_2 = 1$ (see Section SI in the Supporting Information).

Supporting Information

Supporting Information is available from the Wiley Online Library or from the author.

Acknowledgements

This work was supported by the Office of Science, Basic Energy Science, MSE division under grant DE-SC0010467 to CU Boulder. X.Z. acknowledges the support from the National Key Research and Development Program of China Grant No. 2016YFB0700700. The work on calculation of topological properties used the Extreme Science and Engineering Discovery Environment (XSEDE), which was supported by the NSF grant number ACI-1053575. The authors thank Dr. Saicharan Aswartham and Prof. Gang Cao for sharing with them the crystallographic information of the newly synthesized and characterized $BaTeO_3$ ($P2_1/c$) structure, and the authors thank Prof. Dan Dessau for helpful discussions.

Conflict of Interest

The authors declare no conflict of interest.

Keywords

density functional theory, oxide perovskites, structural stability, topological insulators

Received: March 8, 2017
Revised: June 5, 2017
Published online:

[1] C. L. Kane, E. J. Mele, *Phys. Rev. Lett.* **2005**, *95*, 146802.
[2] L. Fu, C. L. Kane, *Phys. Rev. B* **2006**, *74*, 195312.
[3] M. Z. Hasan, C. L. Kane, *Rev. Mod. Phys.* **2010**, *82*, 3045.
[4] Y. Xia, D. Qian, D. Hsieh, L. Wray, A. Pal, H. Lin, A. Bansil, D. Grauer, Y. S. Hor, R. J. Cava, M. Z. Hasan, *Nat. Phys.* **2009**, *5*, 398.
[5] Y. L. Chen, J. G. Analytis, J.-H. Chu, Z. K. Liu, S.-K. Mo, X. L. Qi, H. J. Zhang, D. H. Lu, X. Dai, Z. Fang, S. C. Zhang, I. R. Fisher, Z. Hussain, Z.-X. Shen, *Science* **2009**, *325*, 178.
[6] B. A. Bernevig, T. L. Hughes, S.-C. Zhang, *Science* **2006**, *314*, 1757.
[7] Y. Cao, J. A. Waugh, X. W. Zhang, J. W. Luo, Q. Wang, T. J. Reber, S. K. Mo, Z. Xu, A. Yang, J. Schneeloch, G. D. Gu, M. Brahlek, N. Bansal, S. Oh, A. Zunger, D. S. Dessau, *Nat. Phys.* **2013**, *9*, 499.
[8] T. H. Hsieh, H. Lin, J. W. Liu, W. H. Duan, A. Bansil, L. Fu, *Nat. Commun.* **2012**, *3*, 982.
[9] Z. K. Liu, B. Zhou, Y. Zhang, Z. J. Wang, H. M. Weng, D. Prabhakaran, S.-K. Mo, Z. X. Shen, Z. Fang, X. Dai, Z. Hussain, Y. L. Chen, *Science* **2014**, *343*, 864.
[10] X. Deng, K. Haule, G. Kotliar, *Phys. Rev. Lett.* **2013**, *111*, 176404.
[11] D. J. Kim, J. Xia, Z. Fisk, *Nat. Mater.* **2014**, *13*, 466.
[12] W. A. Harrison, *Electronic Structure and the Properties of Solids: The Physics of the Chemical Bond*, Dover Publications, Inc., New York **1989**.
[13] M. A. Berding, M. van Schilfgaarde, A. Sher, *J. Vac. Sci. Technol., B: Microelectron. Nanometer Struct.–Process., Meas., Phenom.* **1992**, *10*, 1471.
[14] D. West, Y. Y. Sun, H. Wang, J. Bang, S. B. Zhang, *Phys. Rev. B* **2012**, *86*, 121201.
[15] H. Jin, S. H. Rhim, J. Im, A. J. Freeman, *Sci. Rep.* **2013**, *3*, 1651.
[16] B. H. Yan, M. Jansen, C. Felser, *Nat. Phys.* **2013**, *9*, 709.
[17] G. Trimarchi, X. Zhang, A. J. Freeman, A. Zunger, *Phys. Rev. B* **2014**, *90*, 161111.
[18] G. Li, B. H. Yan, R. Thomale, W. Hanke, *Sci. Rep.* **2015**, *5*, 10435.

[19] D. Xiao, W. Zhu, Y. Ran, N. Nagaosa, S. Okamoto, *Nat. Commun.* **2011**, *2*, 596.
[20] S. Okamoto, W. Zhu, Y. Nomura, R. Arita, D. Xiao, N. Nagaosa, *Phys. Rev. B* **2014**, *89*, 195121.
[21] Q. Xu, Z. Song, S. Nie, H. Weng, Z. Fang, X. Dai, *Phys. Rev. B* **2015**, *92*, 205310.
[22] J. L.G. Fierro, *Metal Oxides: Chemistry and Applications*, CRC Press, Boca Raton **2006**.
[23] H. Kawazoe, M. Yasukawa, H. Hyodo, M. Kurita, H. Yanagi, H. Hosono, *Nature* **1997**, *389*, 939.
[24] R. E. Cohen, *Nature* **1992**, *358*, 136.
[25] A. Goldman, *Handbook of Modern Ferromagnetic Materials*, Springer, Boston **1999**.
[26] J. G. Bednorz, K. A. Müller, *Z. Phys. B: Condens. Matter* **1986**, *64*, 189.
[27] *Inorganic Crystal Structure Database*, Fachinformationszentrum, Karlsruhe, Germany **2006**.
[28] L. M. Schoop, L. Müchler, C. Felser, R. J. Cava, *Inorg. Chem.* **2013**, *52*, 5479.
[29] S. M. Young, S. Zaheer, J. C.Y. Teo, C. L. Kane, E. J. Mele, A. M. Rappe, *Phys. Rev. Lett.* **2012**, *108*, 140405.
[30] N. Kumada, N. Kinomura, P. M. Woodward, A. W. Sleight, *J. Solid State Chem.* **1995**, *116*, 281.
[31] S. Kirklin, J. E. Saal, B. Meredig, A. Thompson, J. W. Doak, M. Aykol, S. Rühl, C. Wolverton, *J. Comput. Mater.* **2015**, *1*, 15010.
[32] A. Jain, S. P. Ong, G. Hautier, W. Chen, W. D. Richards, S. Dacek, S. Cholia, D. Gunter, D. Skinner, G. Ceder, K. A. Persson, *APL Mater.* **2013**, *1*, 011002.
[33] S. Terada, H. Tanaka, K. Kubota, *J. Cryst. Growth* **1989**, *94*, 567.
[34] L. G. Wang, A. Zunger, *Phys. Rev. Lett.* **2003**, *90*, 256401.
[35] D. M. Wood, A. Zunger, *Phys. Rev. B* **1989**, *40*, 4062.
[36] H. Raebiger, S. Lany, A. Zunger, *Nature* **2008**, *453*, 763.
[37] Q. Liu, X. Zhang, L. B. Abdalla, A. Zunger, *Adv. Func. Mater.* **2016**, *26*, 3259.
[38] J. P. Perdew, K. Burke, M. Ernzerhof, *Phys. Rev. Lett.* **1996**, *77*, 3865.
[39] G. Kresse, J. Furthmüller, *Comput. Mater. Sci.* **1996**, *6*, 15.
[40] G. Kresse, D. Joubert, *Phys. Rev. B* **1999**, *59*, 1758.
[41] R. Yu, X. L. Qi, A. Bernevig, Z. Fang, X. Dai, *Phys. Rev. B* **2011**, *84*, 075119.
[42] L. Fu, C. L. Kane, *Phys. Rev. B* **2007**, *76*, 045302.
[43] J. Heyd, G. E. Scuseria, M. Ernzerhof, *J. Chem. Phys.* **2003**, *118*, 8207; *J. Chem. Phys.* **2006**, *124*, 219906.
[44] C. G. Darwin, *Proc. R. Soc. A* **1928**, *118*, 654.
[45] S. L. Dudarev, G. A. Botton, S. Y. Savrasov, C. J. Humphreys, A. P. Sutton, *Phys. Rev. B* **1998**, *57*, 1505.
[46] T. Ishidate, S. Abe, H. Takahashi, N. Môri, *Phys. Rev. Lett.* **1997**, *78*, 2397.
[47] P. Błoński, J. Hafner, *Phys. Rev. B* **2009**, *79*, 224418.
[48] A. A. Soluyanov, D. Vanderbilt, *Phys. Rev. B* **2011**, *83*, 235401.